Available free online at www.medjchem.com

Mediterranean Journal of Chemistry

Mediterranean Journal of Chemistry **2024**, 14(1), 69-78

Microstructural, structural and piezoelectric properties of nanorod-like ZnO layers deposited by the two-step CBD process

Véronique Bornand

ICGM, UMR 5253, CNRS-ENSCM-UM, 34293 Montpellier cédex 5, France

Abstract: ZnO layers were grown on SiO_2 substrates by Chemical Bath Deposition (CBD) and characterized in terms of morphological, structural, and local piezoelectric properties. The critical factors that allow the oriented growth of ZnO in nanorod configuration were carefully examined to get close-packed <*c*>-oriented nanostructures for local piezoelectric measurements. After the first step, which consisted of creating ZnO-seeded layers on SiO_2 substrates, the development of ZnO nanorods on these homo-buffer layers was more specifically studied through precursor concentration and growth time parameters. Morphological studies by X-ray diffraction and scanning electron microscopy illustrate that a suitable adjustment of these factors (0.025M equimolar solution, 4h-dip coating) resulted in dense nanostructures with hexagonal wurtzite crystalline state. As-grown films exhibited a strong preferential out-of-plane orientation along the polar *c*-axis. Atomic force microscopy in contact mode (Electrostatic Force Microscopy or EFM) was used to determine the effective piezoelectric coefficient (d_{33}) of such 1D-textured nanosystems. Values around 9.5 pm/V could be measured.

Keywords: Zinc oxide; Chemical bath deposition; Thin films; Nanorods; Self-organized oriented growth; Piezoelectric properties.

1. Introduction

ZnO is a multifunctional material with versatile mechanical, chemical, optical, electrical, and piezoelectric properties and chemical stability [1,2]. If many searches have already been devoted to ZnO, the material is still the subject of attention regarding its attractive and environmentally friendly properties. ZnO nanostructured films can potentially be integrated into various devices, including sensors, actuators, SAW devices, and high-frequency acoustic transducers [3-10]. Even though ZnO shows lower piezoelectric performances than PZT-based materials, $LiNbO_3$ or $LiTaO_3$, the control of both growth and morphology is easier to achieve. For these applications, control of crystalline quality and oriented growth along the polar *c*-axis is a crucial issue, as these properties play a significant role in the performances of the devices [11]. Numerous chemical and physical techniques have recently grown ZnO nanostructures 12-19. While physical methods can produce high-quality and single-crystalline nanostructures, these processes generally require high-temperature syntheses and ultra-high vacuum systems.

On the contrary, chemical processes do not require high equipment costs and can be performed at relatively low temperatures. Recently, we have demonstrated that the Chemical Bath Deposition (CBD) coupled with ultrasonic spray pyrolysis (pyrosol) could lead to highly oriented ZnO layers, suggesting their possible integration into complementary MOS systems [18]. In this later work, CBD was used to create a ZnO buffer layer before the growth and simultaneous crystallization of the whole ZnO nanostructures by pyrosol. In the present work, we focus on the lonely CBD technique to optimize the entire deposition procedure, namely precursor concentration and growth time, to get films with dense columnar nanostructures close to nanorods suitable for local piezoelectric measurements.

Morphologies-Properties-Applications relationships are evident when talking about micro- and nanostructures. Various 1D- and 2D- ZnO nanostructures have been studied in the piezoelectric field these last decades, including nanowires, nanorods, and nanosheets [20-25]. The control of the synthesis of ZnO nanostructures and the development of oriented structures is crucial for achieving reliable ZnO-based devices in optoelectronic and piezoelectric areas [26,27]. Several research teams have reported Piezoelectric characterizations for pure ZnO heterostructures and reveal a large discrepancy in the data, as summarized in Table 1 [28-37].

**Corresponding author: Véronique Bornand*
Email address: veronique.bornand@umontpellier.fr
DOI: http://dx.doi.org/10.13171/mjc02403131749bornand

Received June 15, 2023
Accepted July 9, 2023
Published March 13, 2024

Table 1. Non-exhaustive list of reported experimental piezoelectric coefficient d_{33} of ZnO films

Technique	Film thickness (nm)	d_{33} (pm.V^{-1})	Reference
Pulsed Laser Deposition	200	12	[28]
Pulsed Laser Deposition	800	49.7	[29]
Pulsed Laser Deposition	50	25	[30]
RF Magnetron Sputtering	285	5	[31]
RF Magnetron Sputtering	1380	8	[31]
RF Magnetron Sputtering	1000 / porosity	2.62	[32]
RF Magnetron Sputtering	1000 / no porosity	1.12	[32]
RT Electrospray	<100	21.5	[33]
Atomic Layer Deposition	50	3	[34]
Molecular Layer Deposition	60	2.8	[35]
-	400-600	4.41	[36]
Chemical Bath Deposition	-	7	[37]

In particular, the longitudinal piezoelectric coefficient (d_{33}) depends strongly on the growth deposition process, the film thickness and morphology, the presence of pores, or the degree of texturation. A maximum piezoresponse of tens of pm.V-1 has been reported in these heterostructures for oriented or composite films. While piezoelectric characterizations mainly focused on ZnO thin films grown by physical techniques, the literature on the piezoelectric capability and reliability of ZnO nanostructures grown by chemical processes is minimal. This work aims to demonstrate that using a simple, cost-effective deposition method like CBD allows the growth of 1D-textured ZnO layers exhibiting a local piezoelectric activity able to compete with physical techniques requiring more expensive and bulky devices.

2. Experimental

Depositions were performed on SiO_2 glasses. A thin (less than 50 nm) indium thin oxide layer has been preliminary sputtered on silicon substrates. CBD consists of a two-step seeding and solution growth process. The first step consisted of developing ZnO seeds at the surface of the substrate by immersing the slides at room temperature vertically for a short time (typically 20 seconds) in Zinc acetate [0.2M] dehydrate (Aldrich, 99.99%) isopropanol solutions. Diethanolamine (DEA) and distilled water were used as complexing reagents and polymerization activators. The amorphous seeded layers were then annealed at 550°C in air during 1h30 to eliminate any organic species and promote the crystallization of ZnO grains. The whole procedure was repeated 5 times to create enough seeds for the subsequent development of ZnO nanorods on these homo-buffer layers. The solutions for this second step were prepared from Zinc nitrate hexahydrate (Aldrich, 99.99%) and Hexamethylentetramine (HMTA, Sigma-Aldrich)) dissolved in distilled water, with different molar concentrations ranging from 5.10^{-3}M to 10^{-1}M. The coatings were performed in solutions stabilized at 90°C through a double boiler system. The samples were immersed vertically in the chemical bath the whole time, owing to a clamp clipping onto one end of the substrate. Finally, the samples were annealed at 550°C during 1h30 to improve the crystallinity state of the grown layer in terms of peak sharpness, peak intensity, and preferential orientation. For all annealing treatments, samples were introduced directly in the furnace at high temperatures to limit grain coarsening. The effects of precursor concentration and growth time were studied and optimized for the best compromise between homogeneous dense films and nanorod-structured layers. Studied experimental parameters are listed in Table 2.

The structure and the crystallographic changes were followed by X-ray diffraction (XRD) using an X'PERT diffractometer in a full angular range. Scanning Electron Microscopy (SEM, FEI Quanta 200 FEG) and Atomic Force Microscopy in tapping mode (AFM, Bruker Nanoscope dimension 3100 microscope) monitored the morphology and roughness. The piezoelectric activity of the best-nanostructured materials (0.025M equimolar solution, 4h-dip coating) was determined in contact mode with this commercial Atomic Force Microscope (AFM) under ambient conditions using a CoCr-coated conductive tip with 63.63kHz resonance frequency.

Table 2. Studied experimental parameters (step 2)

Step 1	Zn-acetate :0.2 mo l/l + Isopropanol + Diethanolamine + H_2O	→	Coating (at T_{room}) 5 layers / 20s each + Post-annealing (1h/550°C)	⇨	SEED LAYER
Step 2	Zn-nitrate : **5.10^{-3} to 10^{-1} mol/l** + Hexamethylenetetramine + H_2O	→	Coating (at 90°C) Time: **15 min to 35h** + Post-annealing (1h/550°C)	⇨	NANORODS GROWTH

A significant challenge of EFM piezoelectric measurements is that the tip motion can be due to piezoelectricity, electrostriction, and electrostatic. Using the stiff conductive tip as the top electrode in direct contact with the ZnO surface minimizes the tip-field interaction and avoids electrostatic contributions. The ultra-thin ITO layer before sputtering on SiO_2 ensures the role of an oxide-based conductive bottom electrode. Besides, Pt electrodes were deposited onto one end of the substrate (between the top of the nanorods and the substrate's non-coated area) to release residual space charges that could form at the surface of the samples and avoid short circuits. The applied AC voltage frequency was maintained at 4 kHz while its amplitude (peak-to-peak potential) was varied up to ± 5 V. The 4 kHz frequency is above most noise frequencies and below the tip resonance. A schematic of the ZnO samples prepared for piezoelectric measurements is shown in Figure 1.

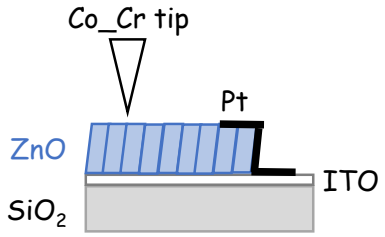

Figure 1. Schematic of the ZnO samples as prepared for piezoelectric measurements

3. Results and discussion

Controlling the nucleus density, size, and distribution on a foreign surface is often difficult. A homo-buffer layer is thus essential to improve the adherence of the subsequent layer and assist the growth of well-organized and preferentially oriented ZnO nanostructures. Growth on substrates pre-coated by ZnO nanoparticles as crystal seeds is much easier as it can effectively lower the interface energy between the crystal nuclei and the substrate, decrease the nucleation barrier [38], and decrease the lattice mismatch between the substrate and the layers to be deposited.

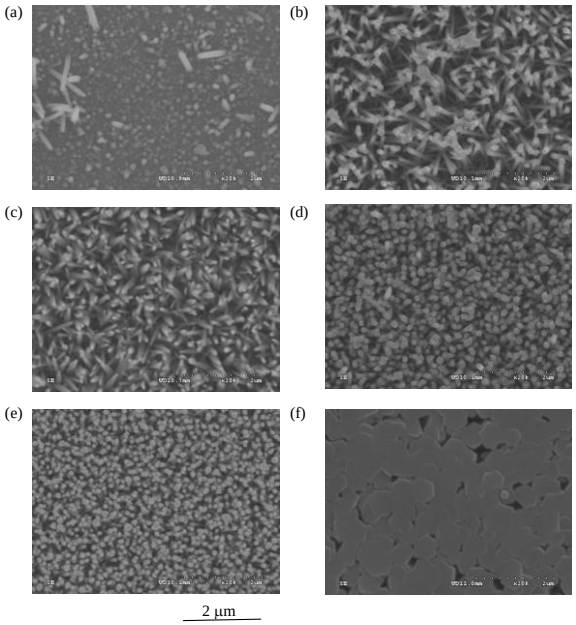

Figure 2. SEM images of ZnO films deposited on ZnO-seeded SiO_2-glass substrates as a function of Zn-nitrate concentration. Results after a 4h-coating at 90 °C and a final annealing at 550 °C during 1h30. Zn-nitrate **(a)** 10^{-3} mol.l^{-1} **(b)** $5*10^{-3}$ mol.l^{-1} **(c)** 10^{-2} mol.l^{-1} **(d)** $2.5*10^{-2}$ mol.l^{-1} **(e)** $5*10^{-2}$ mol.l^{-1} **(f)** 10^{-1} mol.l^{-1}

Furthermore, adjusting the concentration of the precursor solutions in the second step of the CBD process appeared to be an effective way to control the nanostructure evolution on these pre-treated substrates.

Figure 2 shows the surface morphology of ZnO materials deposited on seeded SiO_2 glasses after 4h-coating as a function of Zn concentration. In all cases, layers consisting of uniform and vertically grown particles could be obtained. However, as the concentration increased, the diameter of the crystallites became more extensive, and the heterostructures evolved from small clusters to arrays (70nm in average diameter) and, finally, larger crystallites (up to 500nm in average diameter). Note that all the top surfaces were hexagonally shaped for all samples, in good accordance with the wurtzite ZnO nature revealed by XRD.

The morphology of ZnO layers coated on pre-seeded ZnO/SiO_2 substrates depended strongly on the precursor concentration (Figure 3). The growth rate of ZnO particles increased both laterally and vertically with precursor concentration. The relationship was, however, not linear (Table 3). For the lowest concentrations, ZnO layers showed a granular structure composed of tiny grains with residual porosity, thus suggesting a preeminent vertical growth. While increasing the concentration, vertically aligned densely-packed nanorods could be obtained, indicating the grains' lateral growth rate could be enhanced with increased concentrations. However, film roughness was drastically improved for the highest concentration due to grain coarsening. A concentration of Zn-nitrate of 0.025M appeared as a good compromise for obtaining vertically aligned dense-packed ZnO nanorods.

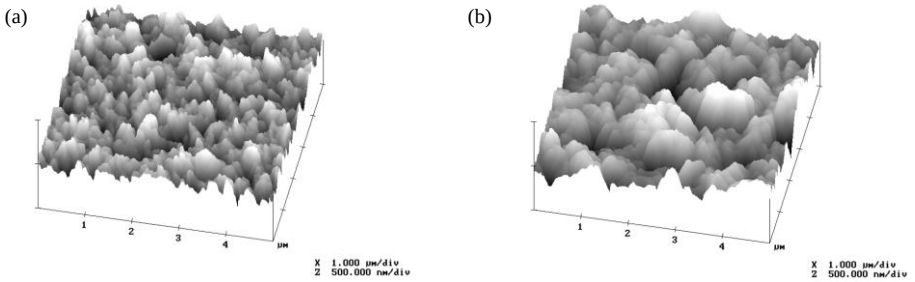

Figure 3. AFM images of ZnO films deposited on ZnO-seeded SiO_2-glass substrates as a function of Zn-nitrate concentration. Results after a 4h-coating at 90°C and a final annealing at 550°C during 1h30. Zn-nitrate **(a)** 0.025 mol.l^{-1} **(b)** 0.1 mol.l^{-1} (X: 1µm/div; Z: 500 nm/div)

Table 3. Morphological properties of ZnO films deposited on ZnO-seeded SiO_2-glass substrates as a function of Zn-nitrate concentration. Results after a 4h-coating at 90°C and a final annealing at 550°C during 1h30.

Zn nitrate (mol.l^{-1})	Thickness (µm)	Grain diameter (nm)	Roughness (nm)
0.01	0.45	50	8
0.025	1	70	24,2
0.1	2.1	500	82

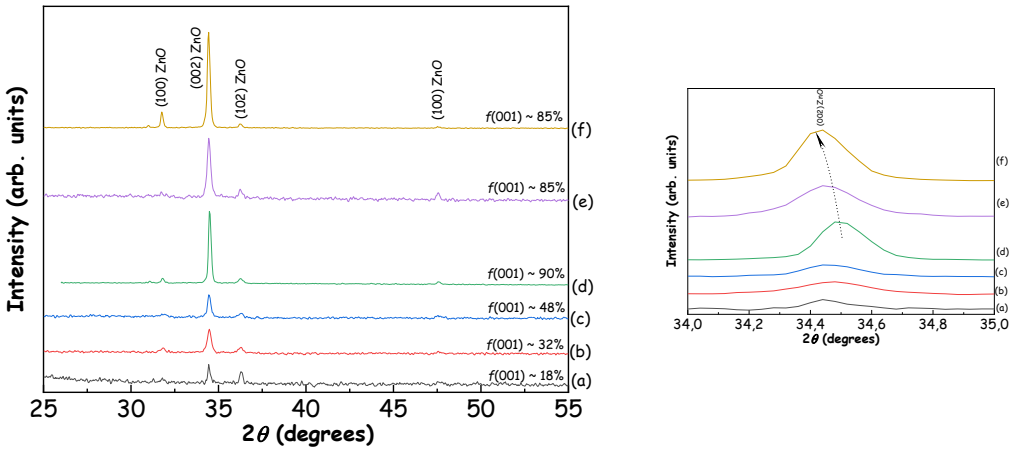

Figure 4. Room-temperature XRD pattern of ZnO films deposited on ZnO-seeded SiO_2-glass substrates as a function of Zn-nitrate concentration. Results after a 4h-coating at 90 °C and a final annealing at 550 °C during 1h30. Zn-nitrate **(a)** 10^{-3} mol.l^{-1} **(b)** 5*10^{-3} mol.l^{-1} **(c)** 10^{-2} mol.l^{-1} **(d)** 2.5*10^{-2} mol.l^{-1} **(e)** 5*10^{-2} mol.l^{-1} **(f)** 10^{-1} mol.l^{-1}

XRD was performed on those ZnO samples as a function of concentration (Figure 4). Polycrystalline materials with the ZnO wurtzite structure could be observed in each case. For the lowest concentration, no preferential orientation could be achieved in link with the sparse development of the ZnO crystallites observed by SEM. By increasing the concentration of the chemical batch, the preferential orientation along the polar *c*-axis can be improved, highlighted by the increase of the Lotgering factor *f*(001). This is in good agreement with the upper-described SEM experiments that evidenced a morphological evolution of the nanostructures towards nanorod-like layers for increasing concentrations. The best results could be obtained for a Zn-nitrate batch of 0.025M. No further improvement of Lotgering factor f(001)could be achieved for upper concentration. Furthermore, the position of the (0002) is shifted to lower angles. This could be explained by an elongation along the c-axis of the wurtzite structure and in-plane contraction due to microstrains in the layers. As revealed by SEM and AFM experiments, the increase of the grain coarsening and grain density in these deposition conditions could explain these results.

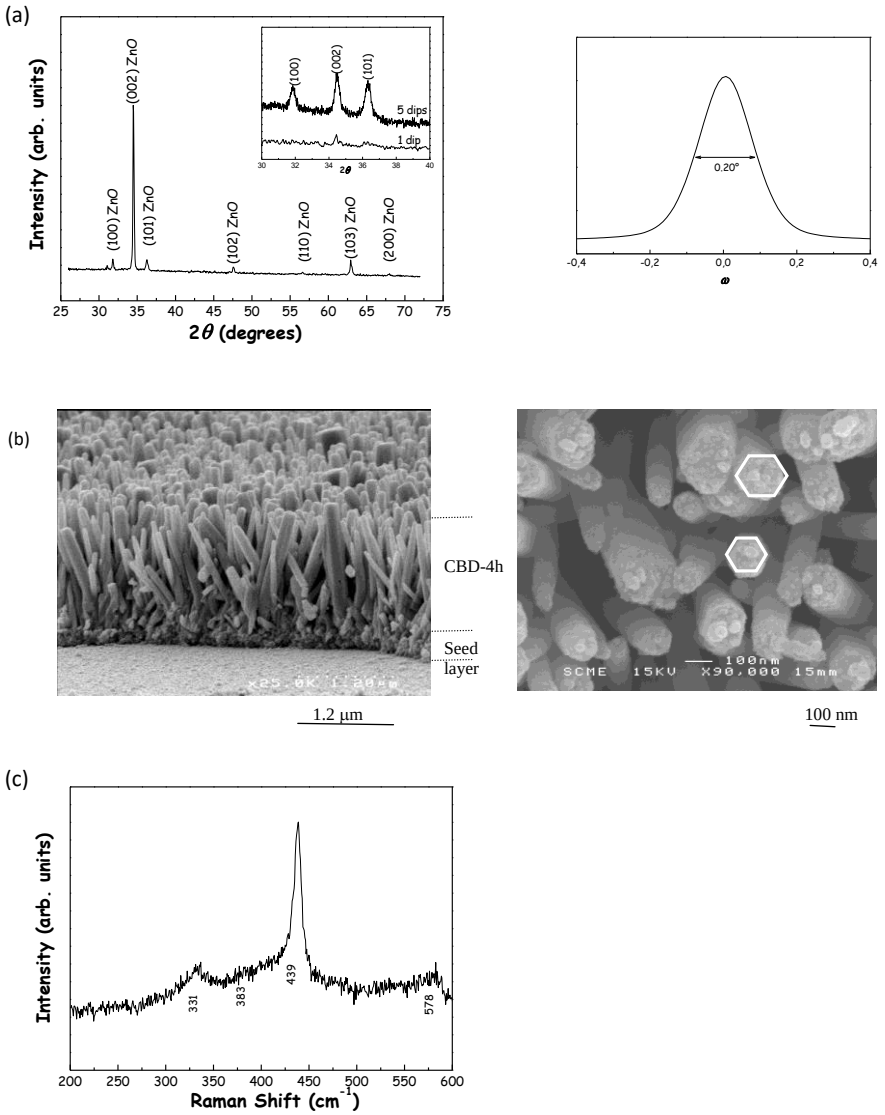

Figure 5. ZnO nanorods deposited on ZnO-seeded SiO_2-glass substrates during 4h. Coatings were performed at 90 °C in a 0.025 M equimolar solution of Zn-nitrate and HMTA, followed by a final annealing at 550 °C during 1h30. **(a)** Room-temperature XRD pattern (inset shows XRD scans of the pre-seeded substrate) and rocking curve analysis around the (001) peak diffraction (right) **(b)** Cross-sectional and surface SEM images (c) Room-temperature Raman spectrum

Self-organized *c*-oriented ZnO nanorods could be developed on SiO_2 substrates (Figure 5). XRD pattern (Figure 5a left) and rocking curve analysis (Figure 5a right) are consistent with a polycrystalline thin film exhibiting a strong <001>-preferential growth as shown by the high value of the Lotgering factor *f*(001) around 90%. This preferential orientation along the <*c*>-axis of the wurtzite structure is further supported by the FWHM (Full Width at the Half Maximum) of the (001) diffraction

peak around 0.2° in the rocking curve. A <111>-oriented Si wafer taken as a reference shows an FWHM of 0.13° in the same configuration. In addition to XRD experiments, the wurtzite ZnO structure was confirmed by Raman spectroscopy by identifying the mode E_2 (high) located at 439 cm^{-1} (Fig. 5c) [39,40]. Two tiny peaks at 331 cm^{-1} and 381 cm^{-1} have been assigned to E_2H-E_2L (multi-phonon process) and A_1T modes, respectively. A small shoulder around 578 cm^{-1} in the spectrum has also been observed and assigned to E1L mode, generally associated with impurities or structural defects. The weakness of this peak suggested the good quality of the synthesized ZnO nanorods on pre-seeded SiO_2 glasses.

The hexagonal wurtzite structure of ZnO confers its piezoelectric and polar character along the *c*-direction. So, in comparison with a non-polar side plane, the growth rate along the polar (0001) crystal plane is relatively fast. Both the relatively high density of the pre-seeded layer and the suitable 0.025 M Zn concentration in the second step of the CBD process could limit the lateral growth of the crystallites. Development of the nanorods seemed to follow a two-growth regime. The surface morphology of the underlying layer was mainly formed by small grains (Figure 2). As the deposition time increases, density is enhanced, with grains growing continuously in lateral size and height. The lateral speed rate could be estimated from SEM micrographs around 7 $nm.h^{-1}$ while the vertical growth rate approaches 250 $nm.h^{-1}$. The second regime was mainly associated with the thickness development of the structure while the diameter of the nanorods was kept constant. The diameter of the nanorods could be quickly controlled around 70 nm after 4h deposit while the thickness of the nanostructures increased linearly with increasing deposition time (Figure 6). Extending the growth time beyond 15h (corresponding to ~4 µm-thick layers) decreased the preferential orientation. This was concurrent with the forming of unorganized and thinner ZnO arrays on top of the film's surface. This third growth regime observed for long-time depositions could be explained by the drastic reduction of reagents in the solution disturbing the nanorods' initial homogeneous and oriented growth.

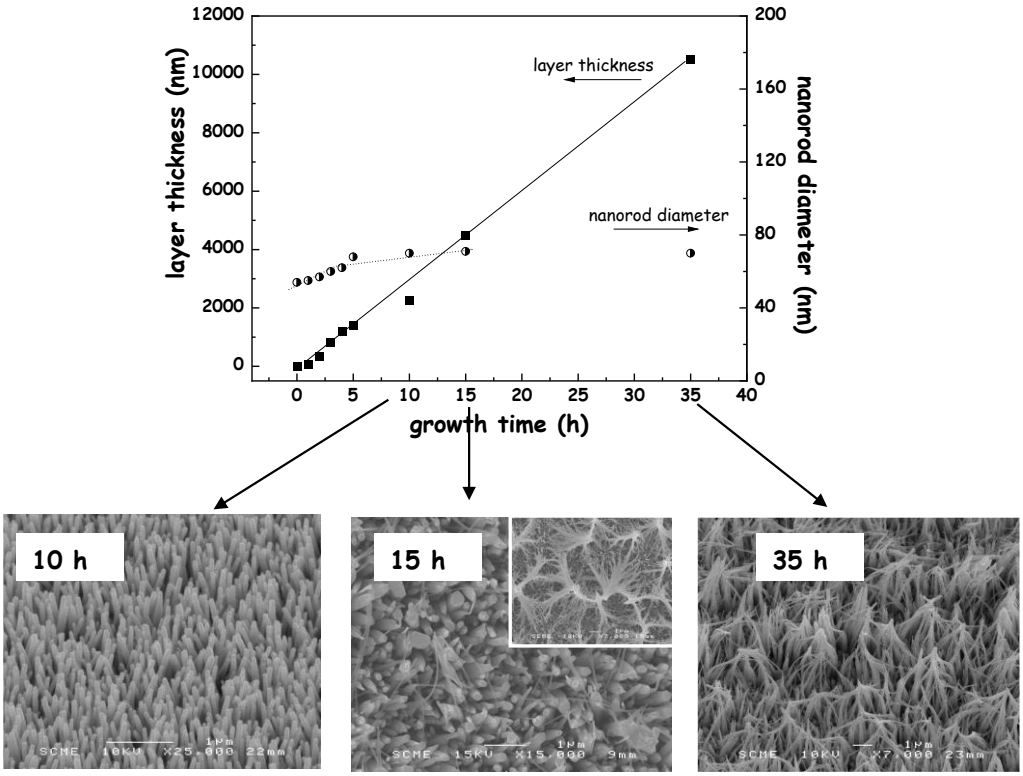

Figure 6. Influence of the deposition time during the 2nd step of the CBD process on the growth of ZnO nanorods on ZnO-seeded SiO_2-glass substrates (data extrapolated from SEM°. Plane-view SEM images of ZnO nanorods deposited on ZnO-seeded SiO_2-glass substrates during 10h, 15h, and 35h

Figure 7 outlines the morphology of ZnO films as a function of deposition times during the second step of the CBD process. The longer the coating, the higher the coarsening of the grains and the higher the mean roughness. Granular and relatively dense morphologies were observed for the shortest deposition times (<5h). The lateral size increased with the growth time. They increased the coating time, which led to less organized structures with rougher surface morphologies linked to an increase along the vertical direction of surface irregularities and second-nucleation phenomena.

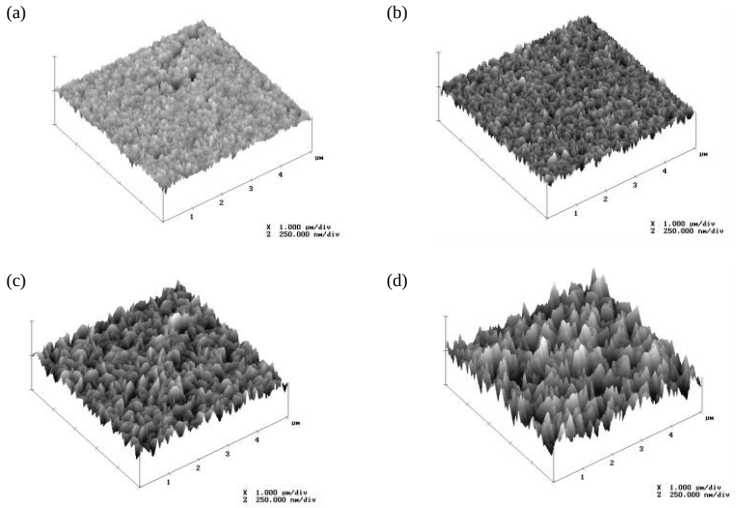

Figure 7. AFM images of ZnO films deposited on ZnO-seeded SiO_2-glass substrates as a function of deposition time during the second step of the CBD process. Results after **(a)** 1h: R_q~8.25 nm **(b)** 2h: R_q~10 nm **(c)** 4h: R_q~24.2 nm (d) 10h: R_q~39.5 nm. (X: 1 µm/div; Z: 250 nm/div)

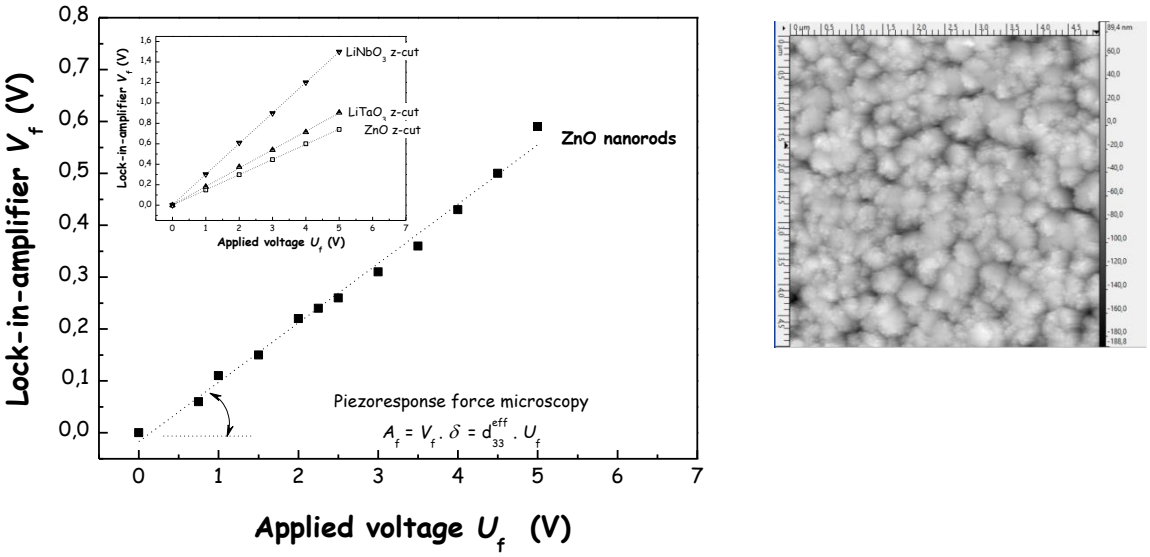

Figure 8. Example of nanoscale piezoelectric measurements of highly *c*-oriented ZnO nanorods deposited on ZnO-seeded SiO_2-glass substrates during 4h (inset shows results for commercial z-cut bulk ZnO, $LiTaO_3$, $LiNbO_3$ crystals), AFM image (on the right side)

The nanoscale Electrostatic Force Microscopy (EFM) resolution was used to check the piezoelectric behavior of our samples and evaluate the effective piezoelectric coefficient d_{33}. The technique allows local potential measurements while mapping the surface. Owing to the inverse piezoelectric effect, the applied voltage induces local oscillations of the layer along the average direction and a height change in tip-to-surface contact. Figure 8 shows the vertical deflection signal of the cantilever (V_f) versus the amplitude of the testing voltage (U_f). A linear response whose slope is directly proportional to the piezoelectric coefficient d_{33} [41,42] could be recorded. In order to ensure the reliability and accuracy of the measurements, experiments were performed in the same conditions on *z*-cut ZnO (d_{33}=12.4 m/V), $LiTaO_3$ (d_{33}=15.1 pm/V), and $LiNbO_3$ (d_{33}=25.2 pm/V) monocrystals. The linear relationship between the lock-in amplifier voltage and the applied voltage is shown in every case, the slope being proportional to the out-of-plane piezoelectric coefficient. Knowing the d_{33} coefficients of these crystals [43,44], we could get the calibration constant of the photodetector sensitivity (δ) and calculate an effective piezoelectric coefficient d_{33} of 9.5 pm/V for *c*-oriented ZnO nanorods deposited on SiO_2 substrates after 4h. Compared to the value for *z*-cut bulk ZnO, the measured results for our nanostructured films are reasonable, confirming the reliability of the CBD process in producing piezoelectric nanosystems. The inherent reduction in the piezoelectric coefficient in nanostructures compared to piezoceramic compounds or crystals is mainly due to size effects as well as to internal

defects in the nanostructured films (possible structural change at the boundary of the nanorods, roughness, substrate effect).

The discrepancy in the piezoresponse of a sample can be mainly attributed to the increment in the film's quality [45]. Beyond the deposition process itself, the grain morphology, the film porosity, the film thickness, the degree of crystallinity, and the preferential orientation are all additional factors that can drastically modify the local piezoelectric properties investigated by PFM [28-37]. A piezoelectric effect can be detected if the polar c-axis is oriented perpendicularly to the applied solicitation. Thus, the piezoresponse is directly influenced by the degree of orientation along the polar c-axis *f*(001) (Figure 9). With increasing deposition times, the d_{33} piezoelectric coefficient can be improved concurrent with enhancing the thin film crystallinity and *c*-preferred growth orientation. However, beyond 4h, the degree of orientation along the polar *c*-axis *f*(001) no longer evolves. It decreases slightly, which could be linked to the surface defect contribution, such as roughness. The d_{33} piezoelectric coefficient follows the same tendency.

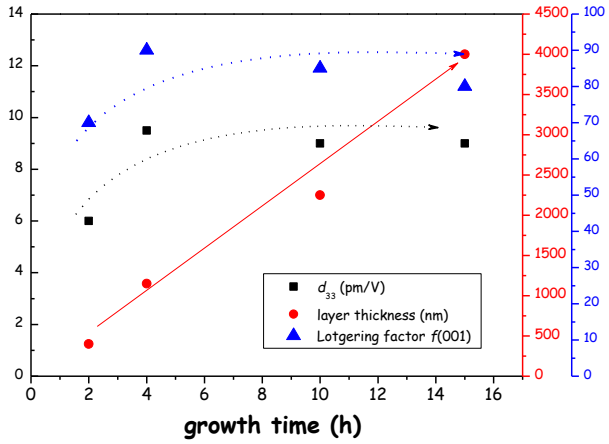

Figure 9. Piezoelectric coefficient d_{33}, Lotgering factor *f*(001), and layer thickness as a function of growth time during the 2nd step of the CBD process. Coatings were performed at 90°C in a 0.025 M equimolar solution of Zn-nitrate and HMTA, followed by a final annealing at 550°C during 1h30

These values are comparable with those reported in the literature for most ZnO nanostructures obtained by physical techniques such as pulsed laser deposition [28,30] or RF magnetron sputtering [31,32]. The proposed CBD process has two main advantages: ease of implementation and cost.

4. Conclusion

Self-organized ZnO nanorods were successfully synthesized on SiO_2 by CBD. The properties of these ZnO nanostructures can be monitored and enhanced by optimizing several parameters, particularly the precursor concentration and growth time during the 2nd step of the CBD process. We demonstrated that a suitable adjustment of the CBD-growth parameters allows the control of density, alignment (preferentially oriented growth), diameter, and length of the nanorods. SEM results demonstrated that the growth of self-organized nanorods could be observed on a pre-seeded SiO_2 substrate with a 0.025 M Zn-nitrate solution for 4h. The wurtzite structure with preferential orientation along the polar *c*-axis could be confirmed by XRD experiments with a Lotgering factor *f*(001) as high as 90%. EFM has been used to evaluate the magnitude of the piezoelectric effect of the best 1*D*-textured materials. Measurements yielded reasonable piezoelectric coefficients of 9.5pm/V for *c*-oriented ZnO nanorods deposited on SiO_2 substrates and provided a quantitative estimation of the piezoresponse of the nanomaterial at the nanoscale. These data approach the values measured for z-cut ZnO crystals, thus making the inexpensive CBD process as competitive as more expensive and bulky physical deposition processes such as pulsed laser deposition.

Acknowledgments

The author wishes to thank F. Fernandez (MEA, Montpellier), L. Daenens (ICGM, Montpellier), and M. Ramonda (CTM, Montpellier) for their helpful technical help in SEM studies, Raman spectroscopy and AFM/EFM experiments, respectively.

References

1- D.K. Sharma, S. Shukla, K.K Sharma, V.A. Kumar, A review on ZnO: Fundamental properties and applications, Mater. Today Proc., **2022**, 49, 3028-3035.
2- P. Sharma, M.R. Hasan, N.K. Mehto, A. Bishoyi, J. Narang, 92 years of zinc oxide: has been studied by the scientific community since the 1930s – An overview, Sens. Int., **2022**, 3, 100182.
3- J.B. Lee, H.J. Lee, S.H. Seo, J.S. Park, Characterization of undoped and Cu-doped ZnO

films for surface acoustic wave applications, Thin Solid Films, **2001**, 39, 641-646.
4- T. Shibata, K. Unno, E. Makino, Y. Ito, S. Shimada, Characterization of sputtered ZnO thin film as sensor and actuator for diamond AFM probe, Sens. Actuators A Phys., **2002**, 102, 106-113.
5- E. Dobrocka, P. Novak, D. Buc, L. Harmatha, J. Murín, X-ray diffraction analysis of residual stresses in textured ZnO films, Appl. Surf. Sci., **2017**, 395, 16-23.
6- Y. Xi, J. Song, S. Xu, R. Yang, Z. Gao, C. Hu, Z.L. Wang, Growth of ZnO nanotube arrays and nanotube-based piezoelectric nanogenerators, J. Mater. Chem., **2009**, 19 (48), 9260-9264.
7- H. Cicek, T. Karacali, H. Efeoglu, B. Cakmak, Deposition of ZnO thin films by rf & magnetron sputtering on silicon and porous silicon substrates for pyroelectric applications, Semiactuators A Phys., **2017**; 260, 24-28.
8- Aminullah, A.K. Kasi, B. Najma, J.K. Kasi, S. Rafique, M. Bokhari, Fabrication of Piezoelectric nanogenerator using 3D-ZnO nanosheets and optimization of charge storage system, Mater. Res. Bull., **2019**, 110711.
9- N. Sinha, S. Goel, A.J. Joseph, H. Yadav, K. Batra, M.K. Gupta, B. Kumar, Y-doped ZnO nanosheets: gigantic piezoelectric response for an ultra-sensitive flexible piezoelectric nanogenerator, Ceram. Int., **2018**, 44 (7), 8582-8590.
10- R. Sha, A. Basak, P.C. Maity, S. Badhulika, ZnO nanostructured based devices for chemical and optical sensing applications, Sens. Actuators Repo., **2022**, 4, 100098.
11- V. Consonni, A.M. Lord, Polarity in ZnO nanowires: A critical issue for piezotronic and piezoelectric devices, Nano Energy, **2021**, 83, 105789
12- L.C. Chao, S.Y. Tsai, C.N. Lin, Vertically aligned ZnO nanowires prepared by thermal oxidation of RF magnetron sputtered metallic zinc oxide, Mat. Sci in Semiconductor Proc., **2013**, 16, 1316-1320.
13- Z. Li, Y. Tang, N. Liao, P. Yang, Study on interfacial between Si and ZnO, Ceramics Int., **2019**, 45, 21894-21899.
14- C. Zandalazini, M. Oliva, J.C. Ferrero, Highly c-axis oriented ZnO thin films on glass substrate by pulsed laser deposition: fluence-dependent effects, J. Nanoelectronics and Optoelectronics, **2019**, 14, 1461-1467.
15- C.H. Kwak, B.H. Kim, S.H. Park, S.Y. Seo, C.I. Park, S. H. Kim, In-situ and ex-situ ZnO-nanorod growth on ZnO homo-buffer layers, J. Cryst. Growth, **2009**, 311, 4491-4494.
16- C.Y. Zhang, X.M. Li, X. Zhang, W.D. Yu, J.L. Zhao, Seed-layer induced growth of high-quality oriented ZnO films by a sol-gel process, J. Cryst. Growth, **2006**, 290, 67-72.
17- T. Dedova, M. Krunks, I. Oja Acik, Hierarchical nanostructures of ZnO obtained by spray pyrolysis, Mat. Chem. Phys., **2013**, 141, 69-75.
18- V. Bornand, A. Mezy, An alternative approach for the oriented growth of ZnO nanostructures, Mater. Lett., **2011**, 65, 1363-1366.
19- A. Kumar, S.K. Saini, G. Sharma, A.K. Sohar, Development and characterization of ZnO thin films for piezoelectric applications, Materials Today: Proceedings, **2020**, 32, 261-263.
20- Y. Xi, J. Song, S. Xu, R. Yang, Z. Gao, C. Hu, Z.L. Wang, Growth of ZnO nanotube arrays and nanotube-based piezoelectric nanogenerators, J. Mater. Chem., **2009**, 19 (48), 9260-9264.
21- A.K. Kasi, B. Najma, J.K. Kasi, S. Rafique, M. Bokhari, Fabrication of Piezoelectric nanogenerator using 3D-ZnO nanosheets and optimization of charge storage system, Mater. Res. Bull., **2019**, 110711.
22- N. Sinha, S. Goel, A.J. Joseph, H. Yadav, K. Batra, M.K. Gupta, B. Kumar, Y-doped ZnO nanosheets: gigantic piezoelectric response for an ultra-sensitive flexible piezoelectric nanogenerator, Ceram. Int., **2018**, 44 (7), 8582-8590.
23- J. Pilz, A. Perrotta, G. Leising, ZnO thin film growth by plasma-enhanced atomic layer deposition: materials properties within and outside the atomic layer, Physica Solidi A, **2020**, 217 (8), 1900256.
24- K.A. Wahid, I.A. Rahim, S.N.A. Safri, A.H. Ariffin, Synthesis of ZnO nanorods at very low temperatures using ultrasonically pre-heated growth solution, Processes, **2023**, 11, 708.
25- S. Abubakar, S.T. Tan, J.Y.C. Lie, Controlled growth of semiconducting ZnO nanorods for piezoelectric energy harvesting-based nanogenerators, Nanomaterials, **2023**, 13, 1025.
26- S. Goel, B. Kumar, A review on piezo-ferroelectric properties of morphologically diverse ZnO nanostructures, J. Alloys Comp., **2021**, 870, 159512.
27- R.K. Pandey, J. Dutta, S. Brahma, C.P. Liu, Review on ZnO-based piezotronics and piezoelectric nanogenerators: Aspects of piezopotential and screening effect, J. Phys. Mater., **2021**, 4, 044011.
28- I.K. Bdikin, J. Gracio, R. Ayouch, Local piezoelectric properties ZnO thin films prepared by RF-plasma assisted PLD method, Nanotechnology, **2010**, 21, 235703.
29- W. Qin, T. Li, Y. Li, J. Qiu, X. Ma, W. Zhang, A high power ZnO thin film piezoelectric generator, Appl. Surf. Sci., **2016**, 364, 670-675.
30- D. D'Agostino, C. Di Giogio, A. Di Trolio, A. Guarino, A.M. Cucolo, A. Vecchione, F. Bobba, Piezoelectricy and charge trapping in ZnO and Co-doped ZnO thin films, AIP Adv, **2017**, 055010.
31- M. Laurenti, S. Stassi, M. Lorenzoni, Evaluation of the piezoelectric properties and voltage

generation of flexible zinc oxide thin films, Nanotechnology, **2015**, 26, 215704.
32- P.C. Lee, Y.L.H. Siao, J. Dutta, R.C. Wang, S.W. Tseng, C.P. Liu, Development of porous ZnO thin films for enhancing piezoelectric nanogenerators and force sensors, Nano-Energy, **2021**, 82, 105702.
33- B. Garcia-Farrera, L.F. Velasquez-Garcia, Ultrathin ceramic piezoelectric films via room-temperature electrospray of ZnO particles for printed GHz devices, ACS Appl. Mater. Interfaces, **2019**, 11, 291676.
34- T. Abu Ali, J. Schäffner, P. Kratzer, Piezoelectric properties zinc oxide grown by plasma-enhanced atomic layer deposition, Phys. Status Solidi Appl. Mater. Sci., **2020**, 217, 2000319.
35- M. Kraüter, T. Abu Ali, B. Stadlober, R. Resel, K. Unger, A.M. Coclite, Tuning the porosity of piezoelectric zinc oxide thin films obtained from molecular layer deposited zircons, Materials, **2022**, 15 (19), 6786-6808.
36- D.A. Scrymgeour, T.L. Sounart, N.C. Simmons, Polarity and piezoelectric response of solution grown ZnO nanocrystals on silver, J. Appl. Phys, **2007**, 101, 014316.
37- M. Fortunato, C.R. Chandraiahgari, G. De Bellis, P. Ballirano, P. Soltani, S. Kaciulis, L. Caneve, F. Sarto, M.S. Sarto, Piezoelectric Thin Films of ZnO-Nanorods/Nanowalls Grown by Chemical Bath, IEEE Transactions On Nanotechnology, **2018**, 17 (2), 311-319.
38- Y. Tong, Y. Liu, L. Dong, Growth of ZnO Nanostructures with Different Morphologies by Using Hydrothermal Technique, J. Phys. Chem. B, **2006**, 110, 20263-20267.
39- K.A. Alim, V.A. Fonoberov, M. Shamsa, Micro-Raman investigation of optical phonons in ZnO nanocrystals, J. Appl. Phys., **2005**, 97, 1-5.
40- A. Khan, J. Pak., Raman Spectroscopic Study of the ZnO Nanostructures, Mater. Soc., **2010**, 4, 5-9.
41- A. Gruverman, O. Auciello, H. Tokumoto, Scanning force microscopy for the study of domain structure in ferroelectric thin films, J. Vac. Sci. Technol. B, **1996**, 14, 602-605.
42- M.H. Zhao, Z.L. Wang, S.X., Mao, Piezoelectric Characterization of individual zinc oxide nanobelt probed by piezoresponse force microscope, Nano letters, **2004**, 4, 587-590.
43- I. Shoji, T. Kondo, A. Kitamoto, M. Shirane, R. Ito, Absolute scale of second-order nonlinear-optical coefficients, J. Opt. Am. B, **1997**, 14, 2268-2294.
44- J.A. Christman, R.R. Woolcott, A.I. Kingon, R.J. Nemanich, Piezoelectric measurements with atomic force microscopy, Appl. Phys. Lett. B, **1998**, 73, 3851-3853.
45- D.L. Cheng, K.S. Kao, C.H. Liang, C.Y. Wang, Y.C. Chen, W.C. Shih, L.P. Chan, Piezoelectric response evaluation of ZnO thin film prepared by RF magnetron sputtering, MATEC web of conferences, **2017,** 109, 04001.